Solar Phys (2012) 281:167–185
DOI 10.1007/s11207-012-0123-5

THE SUN 360

Three-Dimensional Properties of Coronal Mass Ejections from STEREO/SECCHI Observations

E. Bosman · V. Bothmer · G. Nisticò · A. Vourlidas · R.A. Howard · J.A. Davies

Received: 15 November 2011 / Accepted: 4 September 2012 / Published online: 16 October 2012

Abstract We identify 565 coronal mass ejections (CMEs) between January 2007 and December 2010 in observations from the twin STEREO/SECCHI/COR2 coronagraphs aboard the STEREO mission. Our list is in full agreement with the corresponding SOHO/LASCO CME Catalog (http://cdaw.gsfc.nasa.gov/CME_list/) for events with angular widths of 45° and up. The monthly event rates behave similarly to sunspot rates showing a three- to four-fold rise between September 2009 and March 2010. We select 51 events with well-defined white-light structure and model them as three-dimensional (3D) flux ropes using a forward-modeling technique developed by Thernisien, Howard and Vourlidas (Astrophys. J. **652**, 763 – 773, 2006). We derive their 3D properties and identify their source regions. We find that the majority of the CME flux ropes (82 %) lie within 30° of the solar equator. Also, 82 % of the events are displaced from their source region, to a lower latitude, by 25° or less. These findings provide strong support for the deflection of CMEs towards the solar equa-

The Sun 360
Guest Editors: Bernhard Fleck, Bernd Heber, and Angelos Vourlidas

Electronic supplementary material The online version of this article (doi:10.1007/s11207-012-0123-5) contains supplementary material, which is available to authorized users.

E. Bosman (✉) · V. Bothmer
Institute for Astrophysics, University of Göttingen, 37077 Göttingen, Germany
e-mail: ebosman@astro.physik.uni-goettingen.de

V. Bothmer
e-mail: bothmer@astro.physik.uni-goettingen.de

G. Nisticò
Dipartimento di Fisica, Universita della Calabria, 87036 Rende, Italy
e-mail: giuseppe.nistico@fis.unical.it

A. Vourlidas · R.A. Howard
Spaces Sciences Division, Naval Research Laboratory, Washington, DC 20375, USA

J.A. Davies
Rutherford Appleton Laboratory, Chilton Oxfordshire, OX11 0QX, UK
e-mail: jackie.davies@stfc.ac.uk

tor reported in earlier observations, *e.g.* by Cremades and Bothmer (*Astron. Astrophys.* **422**, 307 – 322, 2004).

Keywords Coronal mass ejection

1. Introduction

Since the start of science operations in January 2007, the imagers and coronagraphs of the *Sun-Earth Connection Coronal and Heliospheric Investigation* (SECCHI) suite (Howard *et al.*, 2008), aboard the twin STEREO spacecraft (Kaiser *et al.*, 2008), have provided simultaneous observations of coronal mass ejections (CMEs) from different vantage points in space. Using the white-light synoptic movies provided by the two STEREO/SECCHI/COR2-A and -B coronagraphs, we have compiled a list of 565 coronal mass ejections (CMEs) between January 2007 and December 2010. The CMEs were observed under increasing spacecraft separation angles ranging from about 0° in the early mission phase up to 175° in December 2010. The CME list contains basic information, such as Carrington Coordinates of both spacecraft, CME detection times and position angles, etc. and is available online at the website http://soteria-event.uni-graz.at/.[1] The list was compiled as part of the EU FP7 project SOTERIA (SOlar TERrestrial Investigations and Archives).

A comparison of the monthly average CME rate from the SOTERIA COR2 CME list with the CME rate derived from the SOHO/LASCO CME Catalog[2] yields a very good correspondence for CME events with angular widths greater than or equal to 45°. Thus, the SOTERIA COR2 CME list consists of classic large-scale CMEs, such as analyzed, *e.g.*, by Cremades and Bothmer (2004). Figure 1 shows the comparison of the monthly CME rates from SECCHI and LASCO between January 2007 and December 2010, together with the monthly smoothed sunspot number (SSN) provided by the Solar Influences Data Analysis Center (SIDC)[3] of the Royal Observatory of Belgium. Figure 1 shows that the monthly CME rates and monthly smoothed sunspot numbers show generally similar trends but not detailed correlations as has been reported in earlier studies (*e.g.*, St. Cyr *et al.*, 2000). We note that both the CME and sunspot monthly rates rise by a factor of three to four between September 2009 and March 2010 and remain high in the following months. This increase can be interpreted as the start of the rise of solar activity towards the next solar maximum expected around 2012 – 2013. It is interesting to note that the CME rate remains constant (at 10/month for SECCHI and 7/month for LASCO) for several months in 2009 although the corresponding sunspot number hovers around zero. We investigate the low-coronal source regions of these CMEs using the SECCHI *Extreme Ultraviolet Imager* (EUVI) at 195 and 304 Å. We find that they relate to bipolar photospheric regions of lower magnetic flux and quiescent prominence eruptions, in agreement with the results obtained for the CME source regions studied by Cremades and Bothmer (2004). However, for a number of CMEs, no source region could be identified as in the case of the "stealth CME" reported by Robbrecht, Patsourakos, and Vourlidas (2009). The differences between the CME rates and sunspot

[1] Also available in Tables 1 and 2 in the Electronic Supplementary Material.

[2] CDAW Data Center, Solar Physics Laboratory (Code 671) Heliophysics Science Division, NASA / Goddard Space Flight Center, Greenbelt Maryland, USA: 1996 – 2011, SOHO/LASCO CME Catalog, http://cdaw.gsfc.nasa.gov/CME_list/.

[3] Solar Influences Data Analysis Center, Royal Observatory of Belgium: 2010, Monthly and monthly smoothed sunspot number, http://sidc.oma.be/sunspot-data/.

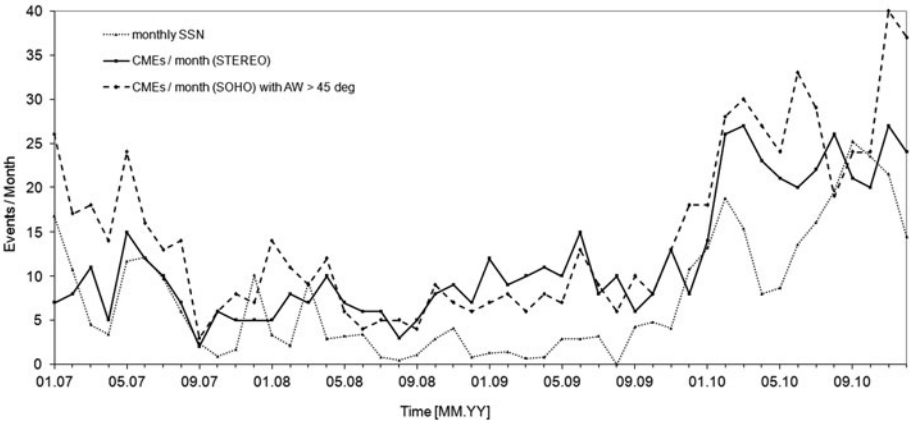

Figure 1 Monthly CME rates observed by STEREO/SECCHI/COR2 (solid line) and those derived from the SOHO/LASCO/C2 CME catalog (dashed line) with an angular width $\geq 45°$ for the time period January 2007 until December 2010. The monthly sunspot number (dotted line) is provided by the SIDC at the Royal Observatory of Belgium. (Solar Influences Data Analysis Center, Royal Observatory of Belgium: 2010, Monthly and monthly smoothed sunspot number, http://sidc.oma.be/sunspot-data/.)

numbers after January 2010 can be explained in terms of decaying active regions of less intense magnetic flux remaining unidentified as sunspots but remaining a source of CME origin, again in agreement with what has been proposed by Tripathi, Bothmer, and Cremades (2004).

From the SOTERIA COR2 list of 565 events, we constructed a "Best-of" list of 120 events based on their clear morphology (judged visually) in the COR2 images. So far, we have fitted 51 of these events as flux ropes with a forward-modeling technique developed by Thernisien, Howard, and Vourlidas (2006) and Thernisien, Vourlidas, and Howard (2009). The flux rope structure is represented by a geometrical construction, called the Graduated Cylindrical Shell (GCS) and is based on the idea that the flux rope morphology can account for the CME white-light observation (Chen *et al.*, 1997; Vourlidas *et al.*, 2000; Cremades and Bothmer, 2004).

In the following sections we give a brief introduction to the GCS Model and a brief presentation of the modeling results and comparisons with the CME source region characteristics.

2. The GCS Model

For the investigation of the three-dimensional (3D) structure of the "STEREO/SECCHI/COR2 Best-of CMEs"[4] the Graduated Cylindrical Shell forward-modeling technique developed by Thernisien, Howard, and Vourlidas (2006) was applied. The geometry and electron density distribution of the GCS flux rope geometry is shown in Figure 2. The GCS geometry consists of two funnel-shaped legs each of length h. The segment h, along the axis through the center of the shell (dash-dotted line), is defined by the center of the Sun, labeled "O",

[4]The complete "Best-of" CME list is shown in Table 3 in the Appendix and in Table 3 in the Electronic Supplementary Material.

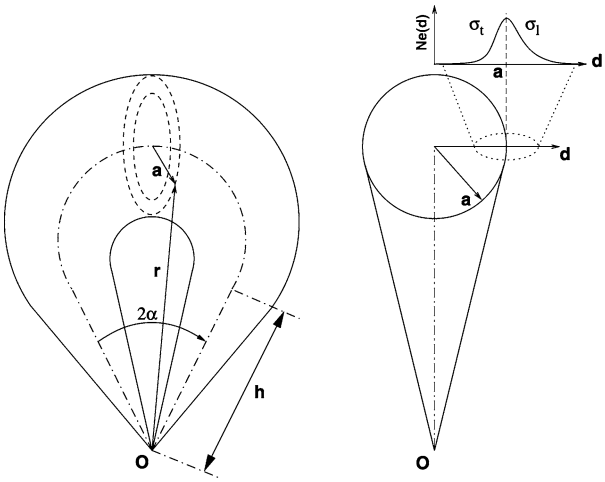

Figure 2 The Graduated Cylindrical Shell Model with a face-on view on the left and an edge-on view on the right. The assumed electron density distribution is shown in the upper right and described with a Gaussian-like function (Thernisien, Howard, and Vourlidas, 2006).

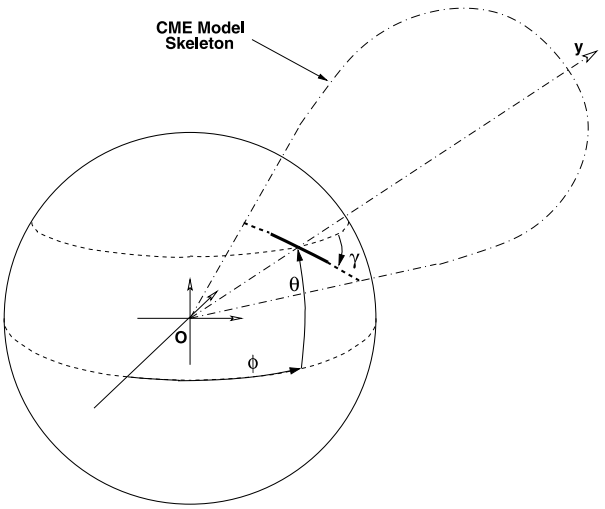

Figure 3 Position and orientation of the GCS Model in 3D Space with the parameters ϕ, θ and γ for the Carrington longitude and heliographic latitude of the apex and the tilt angle, respectively (Thernisien, Vourlidas, and Howard, 2009).

and by the upper end of the cone. The angle between both axes is 2α or α for the half angle, one of the six parameters which define the geometry of the model. The upper part of the model, connecting both legs, is tube shaped. The right image in Figure 2 shows an edge-on view of the model consisting of a circle with the varying radius a for the cross section of the tubelike part and below the tube section the mentioned cone of the legs. As opposed to the length h of the legs h_{front} describes the distance or height between the center of the Sun "O" and the leading edge of the CME. h_{front} can be determined using the parameters h, a, r and α, which are shown in Figure 2.

In order to describe the position and orientation of the flux rope in 3D space the parameters ϕ, θ and γ define the Carrington longitude and heliographic latitude of the apex projection on the solar surface and the tilt angle γ of the source region (SR) neutral line (Figure 3). In this figure the GCS model is oriented normal to the solar surface and located with the projection of the apex on the solar surface at the given (ϕ, θ)-Coordinates where the center of the neutral line of the SR can be found. The legs of the model are located at the

Table 1 Parameters of the GCS Model and the electron density distribution, adapted from Thernisien, Howard, and Vourlidas (2006).

Parameter	[units]	Description
2α	[deg]	Angle between the axis of both legs
h	[r_{sun}]	Height of the legs
h_{front}	[r_{sun}]	Distance from center of the Sun to leading edge
κ		Aspect ratio of a and r
ϕ	[deg]	Carrington longitude of the projection of apex on the Sun's surface
θ	[deg]	Heliographic latitude of the projection of apex on the Sun's surface
γ	[deg]	Tilt angle of the SR neutral line relative to the solar equator
a		Cross section radius of the tube section
r		Distance from center of the Sun to the outer boundary of the shell

opposite ends of the neutral line (NL), which has a tilt angle γ relative to the solar equator. Table 1 provides an overview of the GCS model parameters. Further information regarding the GCS Model can be found in Thernisien, Howard, and Vourlidas (2006) and Thernisien, Vourlidas, and Howard (2009).

3. Examples of GCS Modeling of Events from the "Best-of" List

3.1. CME of 4 August 2009

We apply the GCS model to the CME detected on 4 August 2009 (Figure 4) when the two STEREO spacecraft were separated by 107.5° in heliographic longitude, *i.e.* they observed the CME from different viewing angles. The two STEREO spacecraft detected the CME at different position angles (PA) of 90° and 270°, respectively, as shown in the COR2-A and COR2-B (left) images in Figure 4. The GCS modeling technique was applied to base-difference COR2 images after they had been processed using the standard routines (secchi_prep).[5] For the fit, we selected the time when the CME was the brightest in the COR2 field of view. On 4 August 2009, the CME was modeled when it was observed at 23:22 UT when its leading edge had reached a distance of about 13 solar radii. The right panels in Figure 4 show the modeling results through overlays of the GCS wireframe flux rope geometry on the CME images. The six parameters which describe the geometry of the GCS model are summarized in Table 2.

The synthetic coronagraphic images generated with a ray-tracing code are shown in Figure 5. The ray-tracing code allows us to render the 3D electron density distribution into a coronagraph image taking into account Thomson scattering. In this case, the CME detected in the COR2 field of view is represented by a flux rope which has its apex located at 222° in Carrington longitude lying in the solar equatorial plane (see Table 2). The radial height

[5]Colaninno, R.: 2006 – 2010, The SECCHI_PREP Homepage, *Naval Research Laboratory (NRL/GMU)*, http://secchi.nrl.navy.mil/wiki/pmwiki.php?n=Main.HomePage.

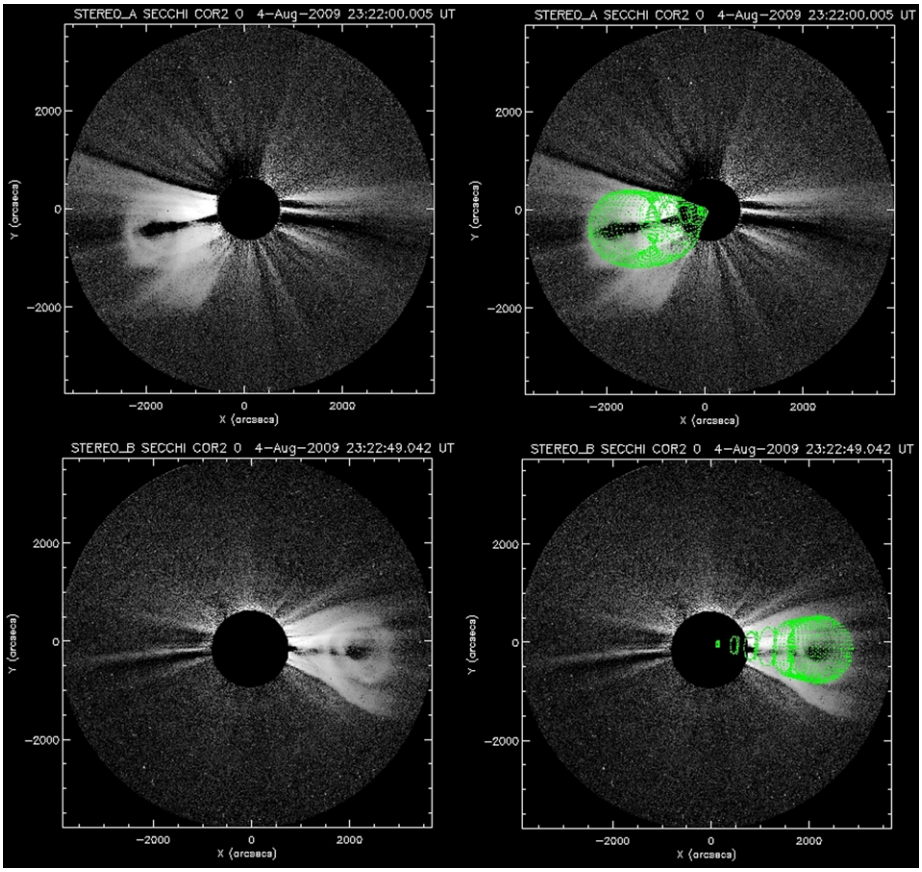

Figure 4 Left column of images: STEREO/SECCHI/COR2-A (top row) and -B (bottom row) white-light coronagraph observations of the CME detected on 4 August 2009 at 23:22 UT. The separation angle between the two spacecraft was 107° in longitude. Right column of images: wireframe rendering results (overlaid in green) derived through the GCS Model.

Table 2 Model results through GCS forward-modeling of two CMEs observed on 4 August 2009 and 1 February 2010.

Parameter		CME 1 (4 August 2009)	CME 2 (1 February 2010)
Longitude	ϕ [deg]	222.5	39.1
Latitude	θ [deg]	−2.8	−18.4
Tilt angle	γ [deg]	0.0	15.1
Height	h_f [r_s]	13.4	16.8
Aspect ratio	κ	0.3	0.3
Half angle	α [deg]	12.0	23.2

of its leading edge is 13 solar radii. Figure 5 further shows the modeled flux rope footpoints and apex locations projected onto the EUVI 195 Å images (right column) for the time of the COR2 modeling. Green crosses signify that the flux rope is located on the visible side of the solar disk whereas white crosses define a backsided flux rope. The white-light structure of

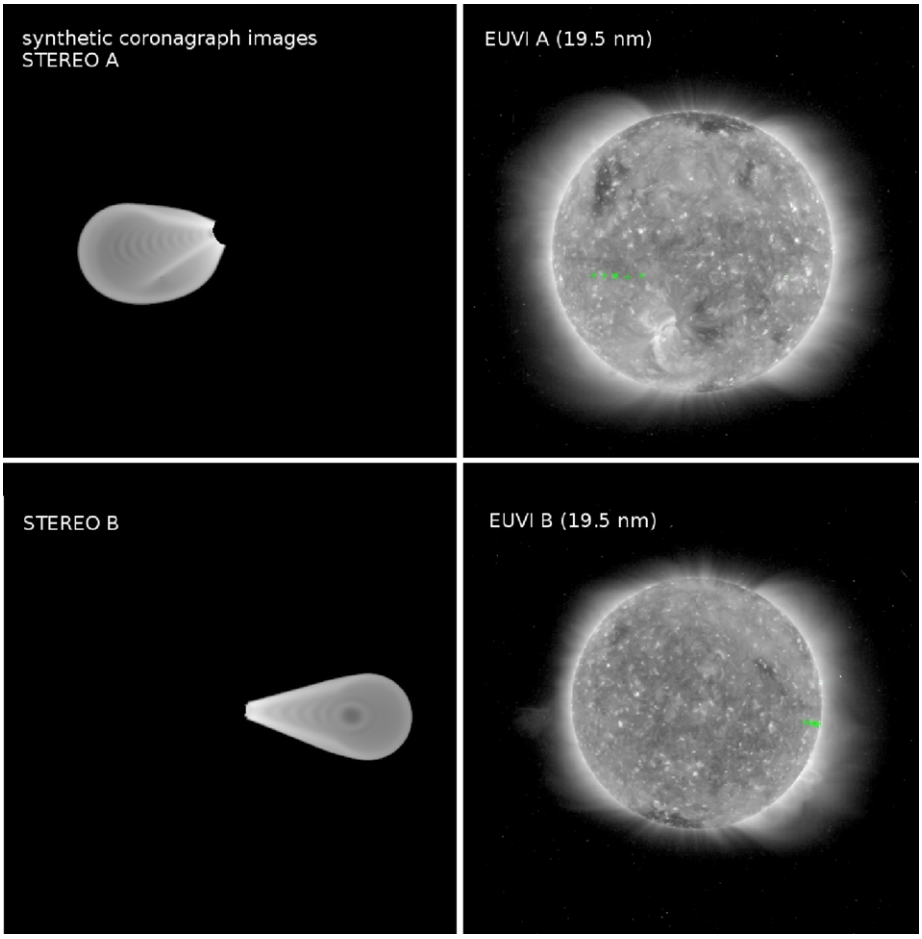

Figure 5 Left column: GCS synthetic coronagraph images for the CME observed on 4 August 2009 at 23:22 UT as shown in Figure 4. The separation angle between the two spacecraft was 107° in longitude. Right column: STEREO/SECCHI/EUVI-A (top) and -B (bottom) observations at 195 Å with projection of the flux rope footpoints and apex on the Sun's surface.

the 4 August 2009 CME reveals features similar to many other cases of the "COR2 Best-of CME" list.

3.2. CME of 1 February 2010

As discussed earlier solar activity as represented by the sunspot number and the monthly rate of CMEs has shown increased levels since about February 2010. In contrast to a CME typical of the solar minimum years, Figure 6 shows a CME detected on 1 February 2010, *i.e.* in the early rising phase of Cycle 24. At this time STEREO-A and -B were separated by 135.3° in heliographic longitude and observed the CME at PAs of about 180° and 225°, respectively. The GCS modeling results are summarized in Table 2. The flux rope parameters fitting this CME differ from those of the 4 August 2009 event. In this case, the flux rope apex was located 18° south of the solar equator and exhibited a tilt angle of 15°. The

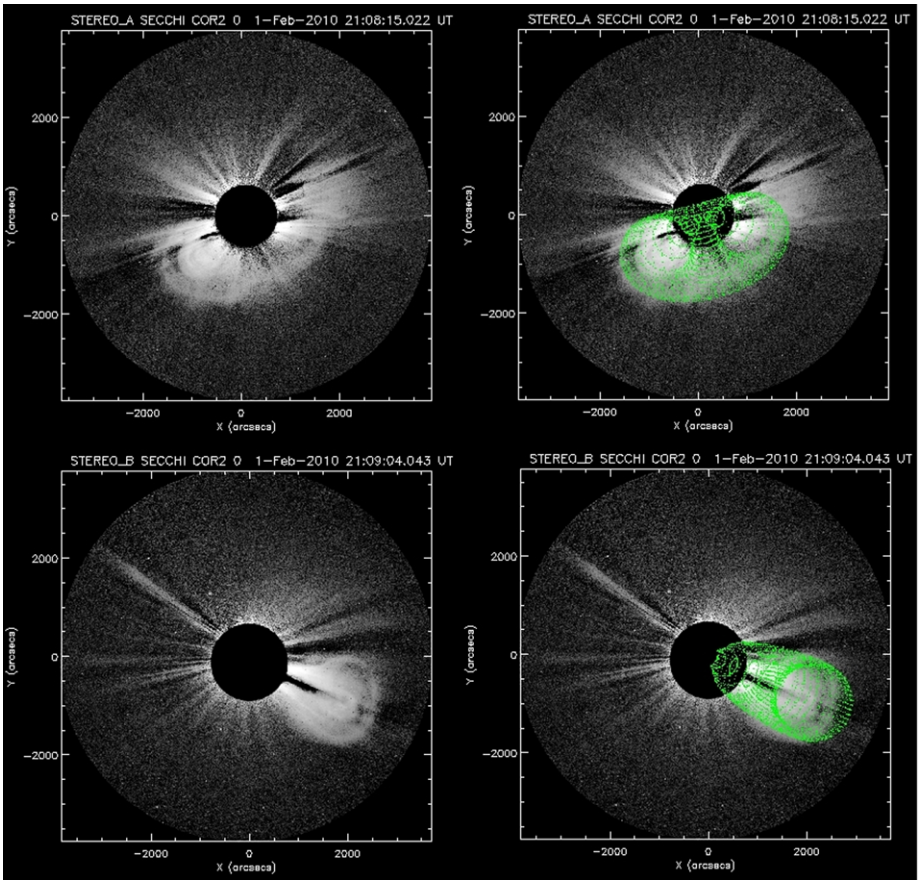

Figure 6 Left column of images: STEREO/SECCHI/COR2-A (top) and -B (bottom) white-light coronagraph observations of the CME detected on 1 February 2010 at 21:08 UT. The separation angle between the two spacecraft was 135° in longitude. Right column of images: wireframe rendering results (overlaid in green) derived through the GCS Model.

angular width was 46°, *i.e.* its calculated half angle of 23° was double the size of the August event. During this time period CMEs generally started looking wider and more massive in white-light coronagraph images. Because of the large angular separation of the COR2-A and -B instruments, the CME looks different in the COR2-A and -B images. The GCS synthetic coronagraphic images generated with the ray-tracing code for this event are shown in Figure 7 together with EUVI-A and -B observations taken at 195 Å.

3.3. GCS Modeling Results for "COR 2 Best-of CMEs"

Out of the 120 events of the "STEREO/SECCHI/COR2 Best-of List"[6] 51 events have been modeled similarly to the sample events described in Sections 3.1 and 3.2. The modeled

[6]The complete "Best-of" CME list is shown in Table 3 in the Appendix and in Table 3 in the Electronic Supplementary Material.

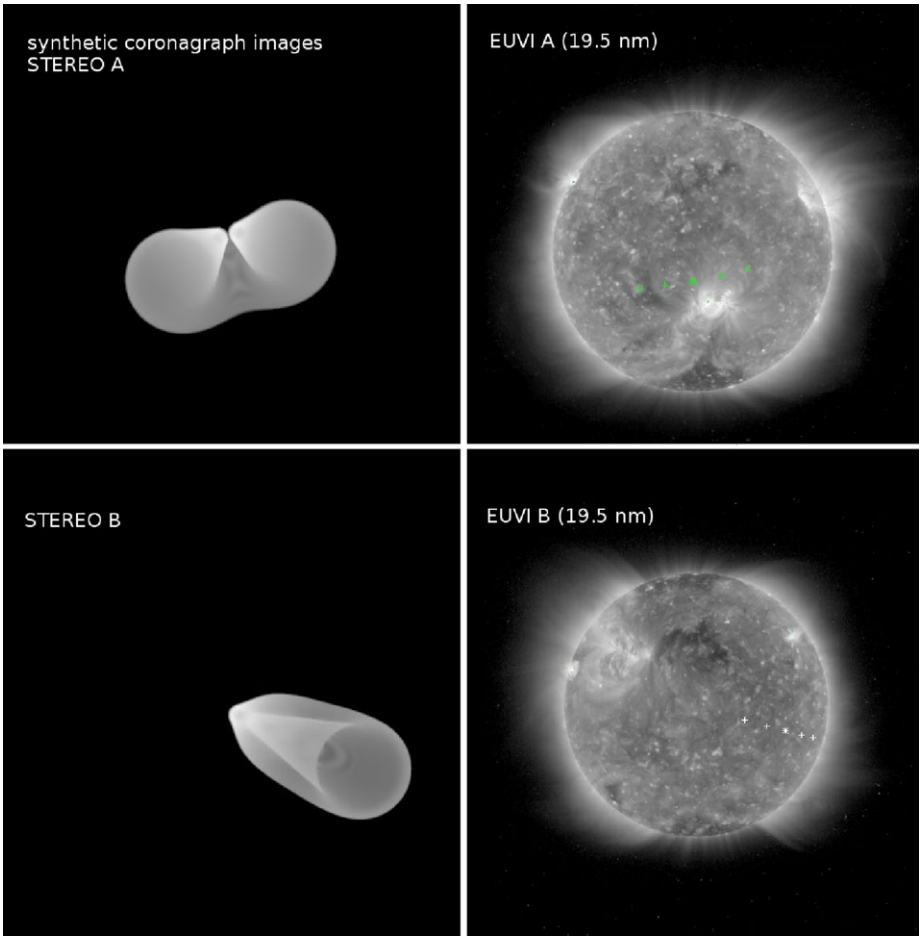

Figure 7 Left column: GCS synthetic coronagraph images for the CME observed on 1 February 2010 at 21:08 UT as shown in Figure 6. The separation angle between the two spacecraft was 135° in longitude. Right column: STEREO/SECCHI/EUVI-A (top) and -B (bottom) observations at 195 Å with projection of the flux rope footpoints and apex on the Sun's surface.

events hitherto were from 2010 because they appeared brighter and were easier to model than the fainter cases appearing at solar minimum. Figure 8 shows the calculated latitudes for 51 flux rope apexes resulting from the modeling of the CMEs in 2010. In 2010 the flux rope apexes were located between 30° southern and 40° northern latitude. Figure 9 shows the calculated GCS flux rope tilt angles plotted versus time in 2010. The tilt angle of a modeled flux rope denotes the angle between the line between its footpoints and apex which are projected on the solar surface and the solar equator. The flux rope is oriented parallel to the equator for an angle of 0° and perpendicular for 90°. The CMEs observed north and south of the solar equator show a similar pattern of scatter in the range of up to 30 – 40°. It is interesting to note that apart from one exception, flux ropes with a tilt angle larger than roughly 40° are lacking. In this context it is important for further studies to inspect the tilt angle of the remaining "Best-of CMEs" observed between 2007 and 2009, because Thernisien, Vourlidas, and Howard (2009) found that *e.g.* the CMEs on 31 December 2007

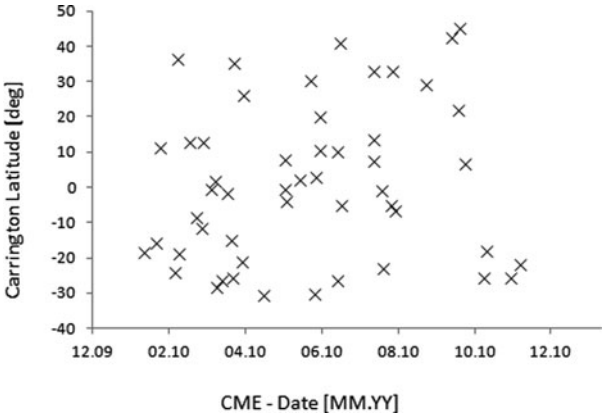

Figure 8 Distribution of latitude of the calculated apex position projected on the solar surface for 51 GCS-modeled CMEs observed in 2010.

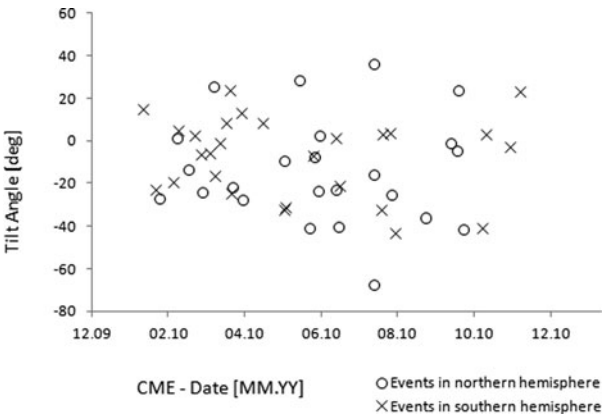

Figure 9 Tilt angle distribution of the line of modeled footpoints and apex projected on the solar surface for 51 GCS-modeled CMEs observed in 2010.

and 23 January 2008 exhibit a large tilt angle of 90° and −49°, respectively. A further investigation of this aspect is needed to understand better the inclination characteristics of flux rope CMEs. Figure 10 shows the distribution of the GCS flux rope half angles α which represents through 2α the separation angle between both legs of the flux rope. The typical half angle of the flux ropes is estimated to lie between 10° and 25° during 2010 for a CME observed between 10 and 15 solar radii. A half angle of 10° to 25° corresponds to an angular width of the CME lying between 20° and 50° which is comparable to the typical angular width of CMEs observed by SOHO/LASCO (*e.g.* St. Cyr *et al.*, 2000; Yashiro *et al.*, 2004).

It should be noted that since the fits are done by hand they exhibit the modeler's subjective understanding of the observed CME. Hence the fit results depend to a certain extent on the experience of the user for the interpretation of the CME white-light observation. In this context Thernisien, Vourlidas, and Howard (2009) used a merit function to determine how well the model is able to reproduce an observed CME's white-light structure. After performing a sensitivity analysis of the model parameters, the authors found that the deviations in the parameters γ and α are an order of magnitude larger than the deviations in the longitude and latitude. Hence the values for the tilt angle may exhibit a larger uncertainty than the one of the other parameters.

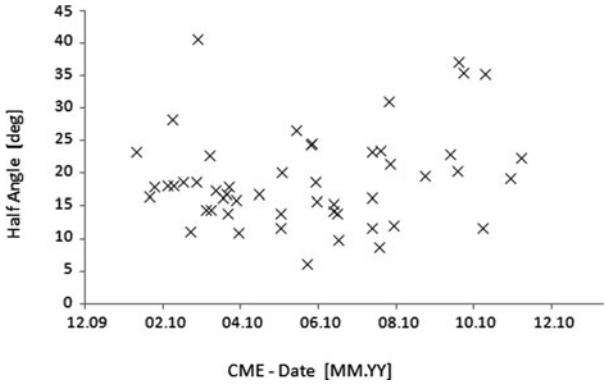

Figure 10 Distribution of the calculated flux rope half angle for 51 GCS-modeled "Best-of CMEs" observed in 2010.

4. Comparison with source region and discussion

To compare the calculated GCS parameters (Table 4) of the flux ropes with the CME associated source region characteristics, we investigated the source region for each CME using SECCHI and SOHO/MDI data. For each modeled CME event we used the SECCHI/COR1 observations to track the CME back towards the low corona and then used the EUVI 195 Å and 304 Å observations to identify the coronal SR.

After identification of a CME's source region we compared the calculated apex position provided by the GCS modeling to the SR location. Figure 11 shows a histogram of the differences between the SR longitude and the modeled apex position in bins of 15° Carrington longitude for 39 events. For the 12 remaining CMEs no associated SRs could be determined. We find that for 82 % (32 out of 39) of the CME events the discrepancy is not larger than 30°. Larger deviations occur only for a small number of events (7 out of 39) and the larger differences are decreasingly frequent. A similar behavior is found for the difference in solar latitude between identified SR and modeled apex position as shown in Figure 12. Here 82 % (32 out of 39) of all CME events exhibit a discrepancy of less than 25° in solar latitude. Considering a 10° difference as insignificant, we can conclude that 41 % of all CMEs do not deflect latitudinally while the rest of the same exhibits a very modest 23° average deflection to lower latitudes.

Next we projected the calculated apexes onto SOHO/MDI (*Michelson Doppler Imager*) Synoptic Charts[7] shown for the CME event observed on 4 June 2010. The center of the observed SR is labeled with a white plus sign and is located within a magnetic bipolar region. For a better visibility the SR is surrounded by a white circle. The radius of the circle is arbitrary with no reference to the spatial extent of the SR. In this case we assume a prominence as the SR, indicated with "P". The position of the apex is marked with a green asterisk and the footpoints with green squares connected with a line which simultaneously denotes the orientation of the flux rope axis. The length of the footpoint line corresponds to the half angle α, respectively, 2α, the angle between both legs of the flux rope. In this case the apex projection lies only 13° south of the identified CME SR with an offset of only 16° in solar longitude. The MDI map reveals a bipolar photospheric region as a source of the analyzed CME as found in the studies of Tripathi, Bothmer, and Cremades (2004). In

[7]Stanford-Lockheed Institute for Space Research, W.W. Hansen Experimental Physics Laboratory (HEPL), Stanford University: 2010, MDI Magnetic Field and Intensity Synoptic Charts, http://soi.stanford.edu/magnetic/index6.html.

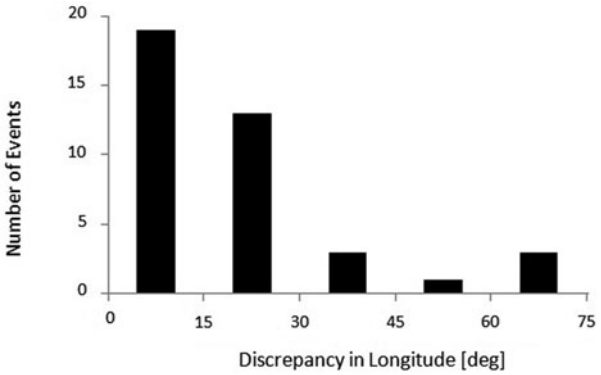

Figure 11 Differences in Carrington Longitude between observed SR and GCS-modeled apex position in bins of 15° for 39 CME events and their associated source regions. For the 12 remaining CMEs no associated SRs could be determined.

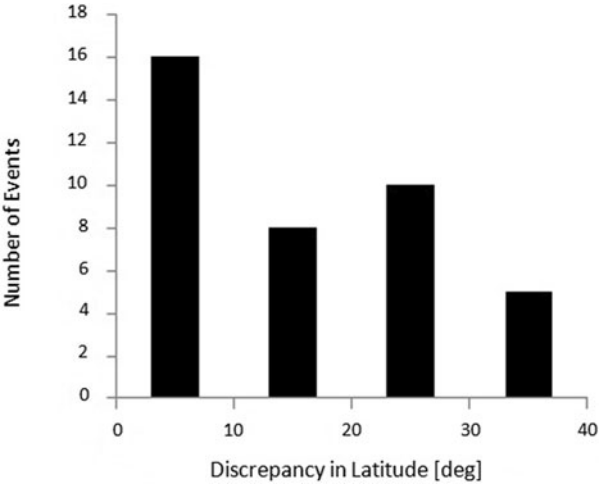

Figure 12 Differences in latitude between observed SR and GCS-modeled apex position in bins of 10° for 39 CME events and their associated source regions. For the 12 remaining CMEs no associated SRs could be determined.

this case also the tilt of the neutral line of the regions of opposite magnetic polarity and the modeled tilt of the flux rope CME, both being of the order 30°, do agree very well.

In contrast to Figure 13, Figure 14 presents an example of a larger discrepancy between the SR latitude and CME latitude for a CME observed on 8 March 2010. In this case the deviation amounts to 37° in solar latitude.

5. Conclusion

In this paper we introduce a CME list[8] based on STEREO/SECCHI/COR2 coronagraph observations. We found that the COR2 CME list is in good agreement with the LASCO CME catalog for events with an angular width greater than or equal to 45°. The COR2 CME list (available online at http://soteria-event.uni-graz.at/) of the EU Seventh Framework Programme project SOTERIA can be considered as a valuable resource of classical large-scale CMEs. We find the monthly CME rates derived by LASCO and SECCHI observations

[8] Available in Tables 1 and 2 in the Electronic Supplementary Material.

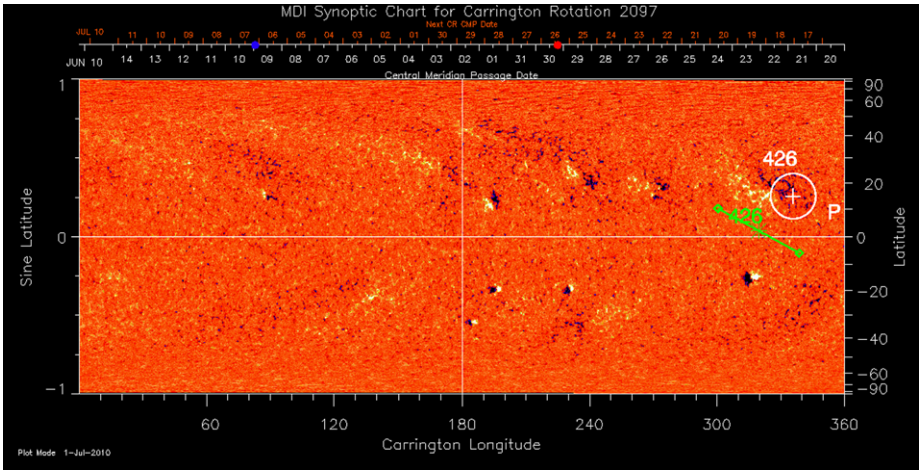

Figure 13 SOHO/MDI Synoptic Chart for Carrington Rotation 2097 labeled with the center of observed SR (white encircled plus sign) and the position of apex and footpoints of the GCS modeled CME observed on 4 June 2010 (green).

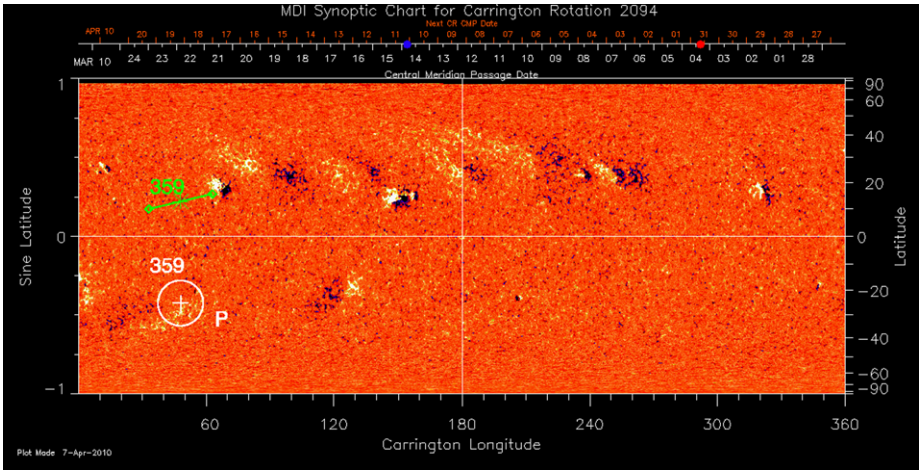

Figure 14 SOHO/MDI Synoptic Chart for Carrington Rotation 2094 labeled with the center of observed SR (white) and the position of apex and footpoints of the GCS modeled CME observed on 8 March 2010 (green).

rise by a factor of 3 to 4 between September 2009 and March 2010. This increase can be interpreted as the start of the overall rise of solar activity towards the next solar maximum expected around the year 2012 – 2013.

From the SOTERIA COR2 CME list we selected 120 events as a "Best-of" list based on their brightness appearance in the COR2 field of view. Fifty-one of the "Best-of CMEs" have been modeled using the GCS forward-modeling technique developed by Thernisien, Howard, and Vourlidas (2006) and Thernisien, Vourlidas, and Howard (2009) to infer the CME's 3D structure. The modeling results reveal:

- A good fit of the observed CME white-light structure as GCS flux ropes.
- The calculated GCS apex latitude position is between 30° southern and 40° northern hemisphere of the solar equator for CMEs observed in 2010.
- The tilt angle for GCS modeled flux ropes is distributed between roughly ±40°.
- The flux rope half angle extends from 10° up to 25° which corresponds to an angular width of the CME lying between 20° and 50°.

From the comparison of the GCS modeled apex position with the identified associated source region position it is found that in 82 % of the CME events the discrepancy extends from 0° up to 30° in Carrington longitude. Larger deviations occurred only for a smaller number of events and the larger differences are also less frequent. A similar behavior is found for the difference in solar latitude between the identified SR and modeled apex positions. Here 82 % of all CME events exhibit a discrepancy of less than 25° in solar latitude. These findings imply that the observed CMEs were commonly deflected away from the radial direction over the first few solar radii.

Some issues which were not discussed in detail in this study but are important and very interesting pertain to error bars of the GCS model parameters. So for example, it should be considered that the deviation for the parameters γ and α are an order of magnitude larger than the deviation for the longitude and latitude. Hence the values for the tilt angle exhibit a larger uncertainty than those for the other parameters (Thernisien, Vourlidas, and Howard, 2009). Further analysis of the calculated GCS flux rope parameters and the investigation of possible CME deflection and CME distortion will be undertaken in the near future.

Acknowledgements The research leading to these results has received funding from the European Community's Seventh Framework Programme (FP7/2007 – 2013) under the grant agreement n° 218816 (SOTERIA project, www.soteria.eu). Volker Bothmer acknowledges support of the project Stereo/Corona by the German Bundesministerium für Bildung und Forschung through the deutsche Zentrum für Luft-und Raumfahrt e.V. (DLR, German Space 59 Agency) as a collaborative effort with the Max-Planck-Institut für Sonnensystemforschung (MPS) under grant 50 °C 0904. Stereo/Corona is a science and hardware contribution to the optical image package SECCHI, developed for the NASA STEREO mission. The STEREO/SECCHI data used for this study are prepared by an international consortium of NASA Goddard Space Flight Center (USA), Lockheed Martin Solar and Astrophysics Lab (USA), Naval Research Laboratory (USA), Rutherford Appleton Laboratory (UK), University of Birmingham (UK), Max-Planck-Institut für Sonnensystemforschung (Germany), Institut d'Optique Thèorique et Appliquèe (France), Institut d'Astrophysique Spatiale (France) and Centre Spatiale de Liège (Belgium). The NRL effort was supported by NASA, the USAF Space Test Program and the Office of Naval Research. The work of Angelos Vourlidas and Russell A. Howard is supported by NASA contract S-136361-Y to the Naval Research Laboratory. Data from the SOHO/MDI instrument are courtesy of the SOHO/MDI consortium. The SOHO/MDI data are produced by an international consortium of the Naval Research Laboratory (USA), Max-Planck-Institut für Aeronomie (Germany), Laboratoire d'Astronomie (France) and the University of Birmingham (UK). SOHO is an international project of collaboration between ESA and NASA.

Appendix

"Best-of CME" List:

Table 3 "Best-of CME" list with 120 CMEs detected with STEREO/SECCHI/COR2- A/B for the time period from January 2007 until December 2010. *No* indicates the CME-Number in the COR2 list, modeled CMEs are marked with *m*. Date and time (*n* stands for next day) corresponds to the observation time with COR2-A and -B, respectively. *PA* denotes the position angle corresponding to the COR2 field of view with 0° pointing to the solar north and increasing angle counter-clockwise. *A* and *B* in the last column indicate how good the CME was visible in COR2-A and -B observations for the user (−− very faint, − faint, + good and ++ very good). *H* stands for Halo and *pH* for partial Halo CME.

No	Date yyyymmdd	Time(A) hh:mm:ss	PA(A) [deg]	Time (B) hh:mm:ss	PA(B) [deg]	Comments
005	20070124	15:02:40	90	15:02:46	90	A++, B−
007	20070130	11:02:40	270	12:02:48	270	A+, B−
020	20070312	00:02:40	90	00:03:01	90	B−, A+
025	20070331	09:52:30	270	09:52:58	270	B+
035	20070509	04:22:30	90	04:53:14	90	A+, B−
038	20070515	19:22:30	45	20:23:17	45	A++, B−
049	20070604	21:22:30	270	03:23:24n	270	A+, B−
050	20070607	20:22:30	225	21:23:25	225	A+, B−
060	20070708	20:22:30	90	21:23:32	90	A+, B−
071	20070821	08:52:30	270	10:53:33	270	A+, B−
078	20071008	17:22:30	270	16:53:22	270	A−, B−
083	20071104	13:52:20	45	20:23:02	45	A+, B−−
086	20071116	10:52:20	225	12:52:57	225	A+, B−−
092	20071231	01:22:20	135	01:52:42	135	A++, B+
093	20080102	10:22:20	90	11:22:41	90	A++, B+
095	20080122	23:52:20	180	23:52:38	135	A+, B+
096	20080129	00:22:20	270	00:22:37	270	A+, B−
100	20080212	07:52:20	225	09:22:36	225	A+, B−
104	20080223	20:52:20	45	17:52:37	45	A+, B−
105	20080227	12:52:20	270	10:22:37	270	A+, B−
107	20080317	15:52:20	270	12:52:40	270	B−, A−−
111	20080325	19:22:20	90	19:52:42	90	A+, B−
113	20080405	16:22:20	270	16:52:45	270	A+, B−
121	20080426	14:52:20	45	15:52:53	315	A+, B−−
125	20080517	10:52:20	90	12:23:01	90	A+, B−−
130	20080601	23:22:20	90	–	–	A+
141	20080731	06:22:20	270	–	–	A−
145	20080908	02:22:20	270	03:53:22	90	A−−, B+
156	20081017	09:52:20	270	10:53:14	90	A−, B+
158	20081026	23:52:20	270	22:23:11	270	A−−, B+
162	20081103	01:22:20	45	01:53:09	315	A−−, B−
167	20081113	16:22:20	225	15:23:06	135	A+, B−
172	20081123	22:22:20	270	04:23:02n	270	A+, B−
175	20081208	17:22:20	315	–	–	A++

Table 3 (*Continued*)

No	Date yyyymmdd	Time(A) hh:mm:ss	PA(A) [deg]	Time (B) hh:mm:ss	PA(B) [deg]	Comments
176	20081212	08:22:20	90	08:22:55	270	A−, B+
179	20081227	06:52:20	45	10:52:50	315	A−, B−−
186	20090114	06:22:00	90	11:22:00	270	A+, B−−
188	20090117	–	–	14:22:24	90	B+
195	20090210	20:52:00	270,90	01:52:19n	225,90	A+, B−−
198	20090218	09:22:00	90	15:22:19	45 – 315	A+, B−−
207	20090316	14:22:00	90,270	12:22:19	90,270	A−−, B+
208	20090318	00:22:00	90	07:22:19	315	A+, B−−
213	20090326	09:22:00	270	19:22:20	135	A+, B+
217	20090410	19:22:00	270	–	–	A+
226	20090423	00:22:00	90,315	00:22:26	90	A+, B−
228	20090502	23:22:00	270	20:22:28	90	A−−, B+
234	20090521	–	–	19:22:35	135	B+
243	20090613	13:52:00	90	14:52:43	270	A+, B−
244	20090615	02:52:00n	90	21:22:43	270	A+, B−
245	20090616	16:52:00	270	16:52:44	270	A+, B−
259	20090723	08:22:00	270	06:52:49	90	A−, B+
262	20090804	18:22:00	90	18:22:49	270	A+, B+
263	20090808	16:52:00	90	22:22:49	90	A+, B−−
264	20090811	14:22:49	90	20:22:00	270	A−, B++
265	20090813	03:22:00	270	–	–	A+
267	20090819	03:08:15	270	05:09:04	90	A+, B−
271	20090903	12:08:15	90	05:09:04	270	A−, B+
288	20091031	05:08:15	90	05:09:04	270	A−, B+
291	20091108	05:08:15	270	06:09:04	45	A++, B−
293	20091115	13:08:15	270	–	–	A−
299	20091121	08:08:15	90	11:09:04	270	A++, B−−
307	20091216	03:08:15	90	04:08:58	270	A+, B−
325m	20100201	23:08:15	135 – 270	22:09:04	225	A−−, B++
333m	20100211	21:08:15	90	23:08:41	270	A−, B++
337m	20100214	08:08:15	45	05:08:40	270	A−, B+
347m	20100225	01:08:15	135,225	02:08:38	225,45	A++, B−
350m	20100228	18:08:15	315	19:08:37	45	A++, B+
351m	20100301	09:08:15	135 – 180	08:08:37	225	A−, B+
359m	20100309	08:08:15	270	12:08:36	90	A+, B−
365m	20100314	13:08:15	225	14:08:36	90	A−, B++
369m	20100319	20:08:15	90	21:08:35	270	A+, B++
370m	20100320	09:08:15	270	11:08:35	315 – 135	A++, B−
373m	20100326	16:08:15	90	17:08:35	270	A−, B+
376m	20100329	12:08:15	270	14:08:35	90	A+, B−
377m	20100330	12:08:15	135,315	14:08:35	45,225	A++, B+
379m	20100403	11:08:15	135	12:08:35	225	A++, B++
383m	20100408	09:08:15	90	07:08:36	270	A+, B−
386m	20100411	09:08:15	225	11:08:36	135	A+, B−

Table 3 (*Continued*)

No	Date yyyymmdd	Time(A) hh:mm:ss	PA(A) [deg]	Time (B) hh:mm:ss	PA(B) [deg]	Comments
387m	20100412	10:08:15	225	13:08:36	135	A−, B−−
389m	20100413	15:08:15	45	14:08:36	315	A−, B++
391m	20100419	05:08:15	135	04:08:36	225	A−, B+
392m	20100419	23:08:15	45	00:08:37n	315	A−, B++
404m	20100506	01:08:15	180	02:08:39	225	A−, B+
415m	20100523	00:08:15	270	00:08:43	90	A+, B−
416m	20100523	21:08:15	90	22:08:43	270	A+, B++
418m	20100524	17:08:15	90	17:08:43	270	A−, B+
426m	20100604	16:08:15	270	16:08:46	90	A+, B++
429m	20100612	16:08:15	45	18:08:49	0	A+, B−
432m	20100615	03:08:15	225,45	04:08:49	135,0	A+, B+
434m	20100616	19:08:15	90	20:08:50	270	A+, B−
435m	20100619	03:08:15	315	04:08:51	45	A+, B−−
437m	20100620	22:08:15	90	23:08:15	270	A−, B−
444m	20100703	07:08:15	270	08:08:55	90	A+, B++
445m	20100703	13:08:15	180,90	14:08:55	225,315	A+, B+
448m	20100705	21:08:15	315	20:08:56	45	A+, B−
449m	20100706	08:08:15	90,360	09:08:56	270	A−−, B+
464m	20100801	04:08:15	90	05:09:04	270	A−, B−−
465a m	20100801	09:08:15	90	10:09:04	315	A+, B++
465b m	20100801	08:08:15	45	10:08:15	315	A−, B−
470m	20100807	20:08:15	90,225	21:09:05	270	A++, B++, H
471m	20100808	17:08:15	225	18:09:06	135	A+, B+
474m	20100814	12:08:15	135	13:09:07	225 – 270	A+, B+, H
476m	20100815	14:08:15	45	16:09:07	315	A+, B−
479m	20100818	06:08:15	45	07:09:08	315	A+, B+
500m	20100911	06:08:15	45,225	07:09:12	315,135	A+, B+
511m	20101001	05:08:15	315	06:09:14	45	A++, B+
515m	20101006	10:08:15	90	14:09:14	270	A+, B+
516m	20101007	15:08:15	0	16:09:14	0	A+, B+
519m	20101011	05:08:15	90	06:09:14	270	A++, B++
525m	20101026	15:08:15	135,315	16:09:14	225,0	A++, B+
528m	20101028	16:08:15	215	15:09:13	90	A++, B++
546m	20101116	14:08:15	135	15:09:11	225	A+, B−
551m	20101124	09:08:15	135	10:09:10	270	A−, B+
552	20101126	00:08:15	225	01:09:10	135	A+, B+
558	20101202	13:08:15	270	16:09:09	90	A−, B−
561	20101206	00:08:15n	135	23:09:08	225	A++, B+
566	20101212	08:08:15	45,135	10:09:06	225,315	A+, B+,pH
568	20101214	18:08:15	45	19:09:06	315	A+, B+
574	20101223	12:08:15	90	13:09:04	270	A+, B+
576	20101226	09:08:15	225	10:09:03	135	A++, B++

One event was found in the synoptic movies subsequently, it was labeled with 465b and the previously found event 465 with 465a.

Fit results of the modeled "Best-of" events:

Table 4 Fit results of the 51 modeled events which are listed in Table 3. *No* indicates the CME-Number in the COR2 list, the six following parameters are the same introduced in Section 2 and summarized in Table 1. The last column denotes the timestamp of the COR2 image used for fitting.

No	ϕ [deg]	θ [deg]	γ [deg]	h_{front} r_{sun}	κ	α [deg]	Time of modeling yyyymmdd-hhmmss
325	39.132	−18.446	15.091	16.786	0.277	23.198	20100201 – 210815
333	219.132	−15.653	−22.919	11.714	0.234	16.491	20100211 – 230815
337	197.888	11.180	−27.392	12.214	0.330	17.888	20100214 – 050815
347	339.876	−24.037	−19.566	13.071	0.336	18.167	20100225 – 000815
350	144.223	36.335	1.118	11.714	0.517	28.229	20100228 – 180815
351	19.008	−19.008	5.031	14.714	0.397	18.167	20100301 – 070815
359	48.074	12.857	−13.415	13.143	0.333	18.726	20100309 – 110815
365	19.008	−8.384	2.236	13.786	0.376	11.180	20100314 – 130815
369	106.211	−11.740	−6.709	13.714	0.385	18.726	20100319 – 200815
370	205.715	12.857	−24.037	12.214	0.597	40.528	20100320 – 090815
373	21.244	−1.118	−39.690	15.000	0.244	9.783	20100326 – 170815
376	126.335	1.678	25.715	11.857	0.388	22.640	20100329 – 120815
377	253.789	−28.510	−16.771	15.000	0.410	14.533	20100330 – 140815
379	258.260	−26.273	−1.118	13.643	0.419	16.491	20100403 – 120815
383	195.653	−1.678	8.383	14.928	0.367	16.211	20100408 – 080815
386	326.459	−15.093	23.477	12.214	0.394	16.771	20100411 – 080815
387	266.087	−25.155	−29.630	13.429	0.244	9.783	20100412 – 110815
389	159.876	35.217	−21.803	14.786	0.499	17.888	20100413 – 150815
391	91.678	−21.242	12.857	13.357	0.514	15.932	20100419 – 040815
392	86.087	26.271	−27.950	15.286	0.622	10.901	20100420 – 000815
404	251.554	−24.597	90.000	15.500	0.665	11.460	20100506 – 020815
415	125.215	−0.560	−32.422	12.072	0.336	11.739	20100523 – 000815
416	320.868	7.826	−9.506	12.857	0.480	13.975	20100523 – 220815
418	304.099	−3.913	−31.304	11.929	0.520	20.123	20100524 – 170815
426	319.752	2.236	28.510	14.429	0.333	26.553	20100604 – 160815
429	336.521	30.186	−40.810	16.286	0.327	6.149	20100612 – 180815
432	228.074	−30.186	−7.267	14.571	0.351	24.317	20100615 – 050815
434	326.459	2.795	−7.828	14.000	0.262	24.595	20100616 – 210815
435	98.381	20.124	−23.477	13.214	0.311	18.726	20100619 – 040815
437	305.219	10.622	2.236	13.714	0.213	15.652	20100621 – 030815
444	346.583	10.062	−22.919	14.928	0.428	14.255	20100703 – 080815
445	205.715	−26.273	1.118	18.072	0.284	15.373	20100703 – 140815
448	320.868	40.806	−40.250	12.643	0.434	13.975	20100705 – 210815
449	134.161	−5.031	−21.242	14.000	0.268	9.783	20100706 – 100815
464	102.856	7.267	36.335	12.000	0.127	11.739	20100801 – 060815
465a	79.380	13.415	−67.640	14.000	0.729	23.198	20100801 – 100815
465b	135.281	32.981	−15.653	4.857	0.271	16.211	20100801 – 100815

Table 4 (*Continued*)

No	ϕ [deg]	θ [deg]	γ [deg]	h_{front} r_{sun}	κ	α [deg]	Time of modeling yyyymmdd-hhmmss
470	324.223	−1.118	−32.422	21.857	0.539	8.663	20100807 – 210815
471	200.124	−22.919	2.795	12.857	0.431	23.478	20100808 – 180815
474	353.293	−5.031	3.353	14.357	0.816	31.025	20100814 – 120815
476	310.806	32.981	−25.155	15.214	0.373	21.522	20100815 – 150815
479	348.818	−6.709	−43.043	16.071	0.717	12.019	20100818 – 070815
500	264.967	22.360	2.795	13.214	0.579	19.565	20100911 – 070815
511	176.645	42.484	−1.118	14.714	0.299	22.919	20101001 – 050815
515	280.620	21.802	−4.471	9.429	0.345	20.404	20101006 – 100815
516	8.942	45.279	23.477	13.214	0.357	37.174	20101007 – 150815
519	225.839	6.709	−41.366	13.571	0.523	35.496	20101011 – 060815
525	69.318	−25.715	−40.810	13.357	0.545	11.739	20101026 – 140815
528	205.715	−17.888	2.795	10.572	0.487	35.217	20101028 – 150815
546	86.087	−25.715	−2.795	12.857	0.382	19.286	20101116 – 150815
551	22.360	−21.803	22.919	13.786	0.397	22.361	20101124 – 090815

References

Chen, J., Howard, R.A., Brueckner, G.E., Santoro, R., Krall, J., Paswaters, S.E., *et al.*: 1997, Evidence of an erupting magnetic flux rope: LASCO Coronal Mass Ejection of 1997 April 13. *Astrophys. J.* **490**, 191 – 194.

Cremades, H., Bothmer, V.: 2004, On the three-dimensional configuration of coronal mass ejections. *Astron. Astrophys.* **422**, 307 – 322.

Howard, R.A., Moses, J.D., Vourlidas, A., Newmark, J.S., Socker, D.G., Plunkett, S.P., *et al.*: 2008, Sun Earth Connection Coronal and Heliospheric Investigation (SECCHI). *Space Sci. Rev.* **136**, 67 – 115.

Kaiser, M.L., Kucera, T.A., Davila, J.M., St. Cyr, O.C., Guhathakurta, M., Christian, E.: 2008, The STEREO mission: an introduction. *Space Sci. Rev.* **136**, 5 – 16.

Robbrecht, E., Patsourakos, S., Vourlidas, A.: 2009, No Trace left behind: STEREO Observation of a Coronal Mass Ejection without low-coronal signatures. *Astrophys. J.* **701**, 283 – 291.

St. Cyr, O.C., Howard, R.A., Sheeley, N.R. Jr., Plunkett, S.P., Michels, D.J., Paswaters, S.E., *et al.*: 2000, Properties of coronal mass ejections: SOHO LASCO observations from January 1996 to June 1998. *J. Geophys. Res.* **105**, 18,169 – 18,185.

Thernisien, A.F.R., Howard, R.A., Vourlidas, A.: 2006, Modeling of flux rope coronal mass ejections. *Astrophys. J.* **652**, 763 – 773.

Thernisien, A.F.R., Vourlidas, A., Howard, R.A.: 2009, Forward modeling of coronal mass ejections using STEREO/SECCHI data. *Solar Phys.* **256**, 111 – 130.

Tripathi, D., Bothmer, V., Cremades, H.: 2004, The basic characteristics of EUV post-eruptive arcades and their role as tracers of coronal mass ejection source regions. *Astron. Astrophys.* **422**, 337 – 349.

Vourlidas, A., Subramanian, P., Dere, K.P., Howard, R.A.: 2000, Large-angle spectrometric coronagraph measurements of the energetics of coronal mass ejections. *Astrophys. J.* **534**, 456 – 467.

Yashiro, S., Gopalswamy, N., Michalek, G., St. Cyr, O.C., Plunkett, S.P., Rich, N.B., *et al.*: 2004, A catalog of white light coronal mass ejections observed by the SOHO spacecraft. *J. Geophys. Res.* **109**(A07105), 1 – 11.